Biomaterials 35 (2014) 9087–9099

Contents lists available at ScienceDirect

Biomaterials

journal homepage: www.elsevier.com/locate/biomaterials

The osteogenic differentiation of SSEA-4 sub-population of human adipose derived stem cells using silicate nanoplatelets

Silvia M. Mihaila [a, b], Akhilesh K. Gaharwar [c, d], Rui L. Reis [a, b], Ali Khademhosseini [e, f, g, h, i], Alexandra P. Marques [a, b], Manuela E. Gomes [a, b, *]

[a] 3B's Research Group – Biomaterials, Biodegradables and Biomimetics, University of Minho, Avepark – Zona Industrial da Gandra, S. Cláudio do Barco, 4806-09, Caldas das Taipas, Guimarães, Portugal
[b] ICVS/3B's – PT Government Associate Laboratory, Braga, Guimarães, Portugal
[c] Department of Biomedical Engineering, Texas A&M University, College Station, TX 77843, USA
[d] Department of Materials Science & Engineering, Texas A&M University, College Station, 77843, USA
[e] Wyss Institute for Biologically Inspired Engineering, Harvard University, Boston, MA 02115, USA
[f] Center for Biomedical Engineering, Department of Medicine Brigham and Women's Hospital, Harvard Medical School, Cambridge, 02139, USA
[g] Harvard-MIT Division of Health Sciences and Technology, Massachusetts Institute of Technology, Cambridge, MA 02139, USA
[h] Department of Maxillofacial Biomedical Engineering and Institute of Oral Biology, School of Dentistry, Kyung Hee University, Seoul 130-701, Republic of Korea
[i] Department of Physics, King Abdulaziz University, Jeddah 21569, Saudi Arabia

ARTICLE INFO

Article history:
Received 19 June 2014
Accepted 23 July 2014
Available online 12 August 2014

Keywords:
Human adipose derived stem cells
SSEA-4$^+$hASCs subpopulation
Silicate nanoplatelets
Osteogenic differentiation
Bone tissue engineering

ABSTRACT

How to surpass *in vitro* stem cell differentiation, reducing cell manipulation, and lead the *in situ* regeneration process after transplantation, remains to be unraveled in bone tissue engineering (bTE). Recently, we showed that the combination of human bone marrow stromal cells with bioactive silicate nanoplatelets (sNPs) promotes the osteogenic differentiation without the use of standard osteogenic inductors. Even more, using SSEA-4$^+$ cell-subpopulations (SSEA-4$^+$hASCs) residing within the adipose tissue, as a single-cellular source to obtain relevant cell types for bone regeneration, was also proposed. Herein, sNPs were used to promote the osteogenic differentiation of SSEA-4$^+$hASCs. The interactions between SSEA-4$^+$hASCs and sNPs, namely the internalization pathway and effect on cells osteogenic differentiation, were evaluated. SNPs below 100 μg/mL showed high cytocompatibility and fast internalization via clathrin-mediated pathway. SNPs triggered an overexpression of osteogenic-related markers (RUNX2, osteopontin, osteocalcin) accompanied by increased alkaline phosphatase activity and deposition of a predominantly collagen-type I matrix. Consequently, a robust matrix mineralization was achieved, covering >90% of the culturing surface area. Overall, we demonstrated the high osteogenic differentiation potential of SSEA-4$^+$hASCs, further enhanced by the addition of sNPs in a dose dependent manner. This strategy endorses the combination of an adipose-derived cell-subpopulation with inorganic compounds to achieve bone matrix-analogs with clinical relevance.

1. Introduction

Bone tissue engineering (TE) requires a readily available source of cells, combined with cell-templates (scaffolds) providing bio-instructive agents (inductive and/or growth factors, cytokines) to trigger and control the osteogenic phenotype and consequently an adequate biological functionality. Osteoinductivity is the key process to induce the differentiation of osteoprogenitor cells into osteoblast cells to eventually form new bone. Thus, extensive research has been focused on determining the appropriate conditions to trigger osteoinductive events. A range of inorganic bioactive materials such as bioactive glasses, calcium phosphates (CaPs) [1], hydroxyapatite (HA), beta tri-calcium phosphates (β-TCP) [2], and orthosilicic acid ($Si(OH)_4$) [3] are exploited as osteoinducers [4]. However, due to their limited processability and insufficient degradation, there is a need to develop a new generation of bioactive materials.

* Corresponding author. 3B's Research Group – Biomaterials, Biodegradables and Biomimetics, University of Minho, Avepark – Zona Industrial da Gandra, S. Cláudio do Barco, 4806-09, Caldas das Taipas, Guimarães, Portugal. Tel.: +351 253 510906; fax: +351 253 510909.
E-mail address: megomes@dep.uminho.pt (M.E. Gomes).

http://dx.doi.org/10.1016/j.biomaterials.2014.07.052
0142-9612/

Recent studies have focused on developing new bioactive materials such as synthetic silicates [5,6] and graphene [7], suggesting unexploited routes for biomaterials design and regenerative medicine. In particular, bioactive silicate nanoplatelets (sNPs) based on synthetic silicate (Laponite, $Na^{+}_{0.7}[(Mg_{5.5}Li_{0.3})Si_8O_{20}(OH)_4]^{-}_{0.7}$) have shown to induce osteogenic differentiation of bone marrow human mesenchymal stem cells (hMSCs) in the absence of osteoinductive factors, such as BMP-2 or dexamethasone [6]. A single dose of these sNPs enhances the osteogenic differentiation of hMSCs, when compared to hMSCs cultured in standard osteogenic differentiation conditions (in the presence of dexamethasone). Moreover, these synthetic silicates have shown to physically interact with both synthetic and natural polymers and can be used as injectable matrices for cellular therapies [8–11]. Although these findings foster the development of new bioactive nanomaterials for bone TE [5,8,12,13], limited availability of bone marrow hMSCs, invasive retrieval procedures and high donor-site morbidity compromise the clinical applicability of the sNPs combined with these cells.

Recently, human adipose derived stem cells (hASCs) isolated from the stromal vascular fraction (SVF) of adipose tissue (AT) have emerged as one of the most promising stem cell populations identified thus far [14,15]. Moreover these cells have the ability to differentiate along multiple lineage pathways as reported in literature [14,15]. From a practical standpoint, human AT is abundant and easily obtained in large quantities with low donor-site morbidity or patient discomfort. The use of autologous hASCs as a research tool and as basis of cellular therapeutic strategies is feasible, making them preferential cells for TE, compared to bone marrow hMSCs. Furthermore, considering the limitations of hASCs in terms of differentiation potential (osteogenic [16], chondrogenic [16], adipogenic [16], myogenic [16] and neurogenic [17]), recent studies have shown that a selected and enriched cellular subset has significantly higher differentiation potential. For instance, STRO-1^{+}hASCs [18], $CD105^{-}$hASCs [19], $CD90^{+}$hASCs [18,20] and $p75^{+}$hASCs [18] were found to exhibit higher osteogenic potential when compared to hASCs. Nonetheless, considering that the majority of biological systems rely on the different cellular interactions, it is important to classify a cell source that can act as starting point for several differentiation pathways. Thus, the isolation of cells from AT is relevant for bone TE and more appealing for clinical translation.

In our previous work [21], we have shown that SVF of the human AT, contains a subpopulation defined by their positive expression of the pluripotency-associated marker, SSEA-4 that is capable of differentiating into mature microvascular-like endothelial cells. Interestingly, this cell subpopulation also showed a superior potential to differentiate towards the osteogenic lineage, compared to hASCs. Therefore, AT can be used as a single cell source to obtain a sub-population of cells, SSEA-4^{+}hASCs, that under specific conditions give rise to endothelial- and osteoblast-like cells, further reinforcing its relevance in designing bone-mimicking constructs.

Herein, we propose to use sNPs to promote and induce the osteogenic differentiation of SSEA-4^{+}hASCs by intracellular interplay, as well as through direct cellular interactions. We hypothesize that the addition of sNPs to SSEA-4^{+}hASCs induces osteogenic differentiation of SSEA-4^{+}hASCs. The combination of cells with high potential towards osteogenic differentiation with inorganic compounds that are able to sustain and improve the extent of mineralization can be a potential avenue towards formation of functional bone tissue. This approach up-holds the promise of developing feasible solutions for the induction of higher levels of new bone formation.

2. Materials and methods

2.1. Hydrodynamic diameter and surface charge of sNPs

Laponite silicate nanoplatelets (sNPs, $Na^{+}_{0.7}[(Mg_{5.5}Li_{0.3})Si_8O_{20}(OH)_4]^{-}_{0.7}$, Rockwood, USA) were dissolved in ultrapure water at different concentrations (<10 mg/mL). The hydrodynamic diameter and zeta potential of the sNPs were measured by photon correlation spectroscopy and laser Doppler anemometry, respectively, using a Malvern Zetasizer Nano ZS (Malvern Instruments, UK). Each analysis was performed at 25 °C, with a detection angle of 90° and a refractive index of 1.5 (for inorganic particles). Each formulation was analyzed in triplicate.

2.2. SSEA-4^{+}hASCs selection and culture

Human abdominal subcutaneous AT samples were obtained from healthy female with an average age of 44 years, undergoing lipoaspiration procedure, after informed consent. The retrieval and transportation of the samples to the 3B's Research Group laboratorial facilities were performed under a protocol previously established with the Department of Plastic Surgery of Hospital da Prelada, Porto, Portugal and approved by the local Ethical Committee. All the samples were processed within 24 h after the surgical procedure, as previously described [21]. Briefly, the AT was digested with 0.05% (wt/v) collagenase II A (Sigma, Germany) in phosphate buffer saline (PBS), for 45 min, under agitation in a shaking bath at 37 °C. The digested tissue was filtered through a 200 μm mesh pore size strain, followed by centrifugation to remove the mature adipocytes and undigested connective tissue. After performing lysis to disrupt the red blood cells, the crude was centrifuged and resuspended in PBS to obtain the SVF.

The immunomagnetic selection of the SSEA-4^{+}hASCs was performed based on the coating of commercially available magnetic beads (Dynabeads® M-450 Epoxy beads, Invitrogen, USA) with SSEA-4 (clone MC813) antibody (Santa Cruz Biotechnology, USA) following the manufacturer's instruction and as previously reported [21]. Briefly, 2×10^7 immunomagnetic beads resuspended with 10 μL of the SSEA-4 antibody at a final concentration of 2 μg/mL, and then incubated, overnight, at room temperature, under gentle stirring. Subsequently, the SSEA-4 coupled beads were separated with a magnet and mixed with freshly isolated SVF in order to select the SSEA-4^{+} cells residing within the cell crude (SSEA-4^{+}hASCs). The cells bonded to the beads were separated from the rest of the cell suspension using the magnet.

The SVF and the SSEA-4^{+}hASCs were both cultured with basal medium (Minimum Essential Medium Eagle-alpha Modification, α-MEM, Gibco, USA), supplemented with sodium bicarbonate (Sigma, Germany), 10% fetal bovine serum (FBS, Gibco, USA) and 1% penicillin/streptomycin (Pen/Strep, 100 U/100 μg/mL, Gibco, USA). When reaching 80% confluence, cells were detached from the culture flasks using TrypLE™ Express (Invitrogen, USA) and kept under the same conditions along the passages. Both cell subgroups were used at passage 2 for further experiments.

2.3. SNPs cytotoxicity screening

The effect of sNPs on cells metabolic activity was investigated by monitoring metabolic activity of adhered SSEA-4^{+}hASCs (passage 2), cultured in basal medium, for a period of 7 days. Cells were seeded in 48-well plates at a density of 2×10^3 cells/cm^2 and sNPs were added to a final concentration ranging from 0 to 2 mg/mL. At preselected time points, cells were washed thoroughly with PBS, and a mixture of serum- and phenol-red free culture medium and MTS reagent (Promega, USA) in a 5:1 ratio, was added to the cells. Samples were incubated for 3 h, after which 100 μL of each sample were transferred to 96-well plates and optical density (OD) at 490 nm was measured on a microplate reader (Synergy HT microplate reader, Biotek, USA). The metabolic activity of the test groups was normalized with the control group (cells without sNPs) to determine the dose response. Aiming at further assessing the effect of the sNPs over cells cytoskeleton organization, cells were fixed with formalin and stained with Phalloidin-TRITC (Sigma, USA) for visualization of the F-actin filaments.

2.4. Assessment of internalization efficiency of sNPs by SSEA-4+hASCs

The sNPs were labeled with rhodamine B prior to assessing their internalization ability. For this purpose, 2 g of sNPs were added to 100 mL of 0.1% (wt/v) of rhodamine B isothiocyanate (Sigma, Germany) solution prepared in anhydrous DMSO, in dark conditions. The mixture was kept under continuous stirring, overnight, at 4 °C. Several washing steps with absolute ethanol were performed in order to separate the sNPs from the organic phase and excess rhodamine B. Finally, sNPs were air-dried and kept at room temperature, protected from light, until further used.

The SSEA-4^{+}hASCs (passage 2) were seeded at a cell density of 2×10^3 cells/cm^2 and allowed to adhere. After 24 h, rhodamine-labeled sNPs (1, 10, 20, 50, 100 and 200 μg/mL) were added to the culture wells and cultures were maintained in basal medium, in the presence/absence of 10^{-6} M colchicine, for additional 24 h. SSEA-4^{+}hASCs cultured in basal medium in the presence of colchicine, but without the sNPs, were used as negative control. Cells were then washed thoroughly with PBS, trypsinized and fixed with acquisition buffer (PBS containing 10% formalin and 0.1% sodium azide) and 10% formalin respectively for analysis in a FACS Calibur flow cytometer (BD Biosciences, USA). In the flow cytometry analysis cells of interest

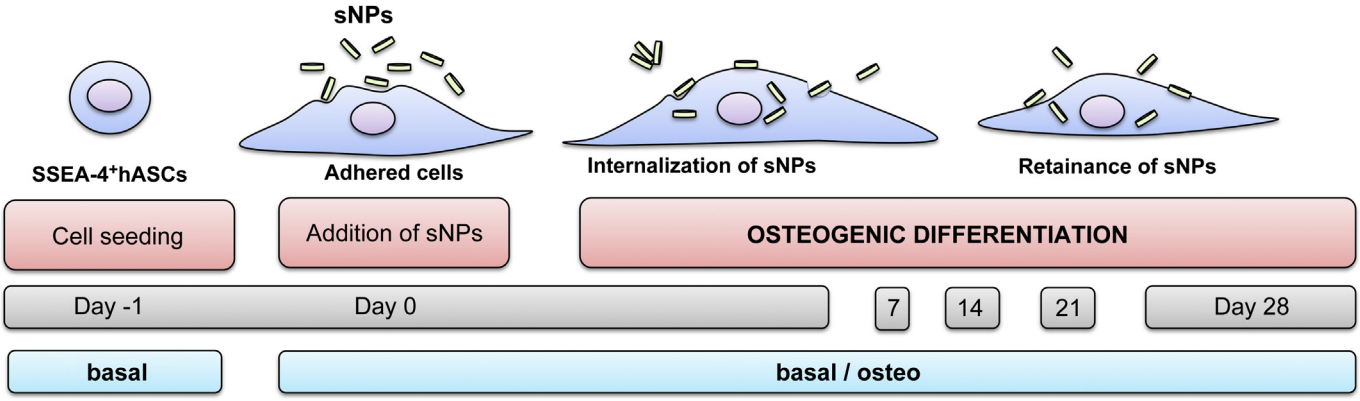

Fig. 1. Experimental setup depicting the temporal approach followed to induce the osteogenic differentiation of SSEA-4$^+$hASCs. After selection from the freshly isolated SVF, SSEA-4$^+$hASCs were cultured in basal medium up to passage 2, then seeded at a density of 2000 cells/cm^2 and allowed to adhere for 24 h until the sNPs were added. Cultures were maintained either in basal medium or under osteogenic differentiation conditions. At pre-selected time points (days 7, 14, 21 and 28) samples were retrieved to assess the extent of differentiation.

were gated in a forward versus side scatter dot plot with a linear scale. Acquired data were displayed as histogram plots created using the CellQuest software (BD Biosciences, USA). Apart from that, for rhodamine samples fixed on coverslips, cell nuclei were counterstained with 4,6-diamidino-2-phenyindole dilactate (DAPI). Samples were visualized and images were acquired using the Axioplan Imager Z1 fluorescence microscope (Zeiss, Germany) and the AxioVision 4.8 software (Zeiss, Germany).

2.5. Osteogenic differentiation

Confluent SSEA-4$^+$hASCs (passage 1) were removed from the culture flasks using TrypLE™ Express (Invitrogen, USA) and seeded at a density of 2×10^3 cells/cm^2 in basal medium. Cells were allowed to adhere and after 24 h, medium was replaced with either sNPs-containing (1, 10 and 100 μg/mL) basal medium or osteogenic medium (osteo) consisting in basal medium supplemented with 10 mM beta-glycerophosphate (Sigma, Germany), 10^{-8} M dexamethasone (Sigma, Germany), and 50 mg/mL L-ascorbic acid 2-phosphate sesquimagnesium salt hydrate (Sigma, Germany). Cells were incubated in a humidified environment at 37 °C with 5% CO_2 for 7, 14, 21, and 28 days, with culture media replenishment every 3–4 days. SSEA-4$^+$hASCs and hASCs cultured in basal and osteo media in the absence of sNPs were used as controls. The experimental setup is depicted in Fig. 1.

2.6. Cell number quantification

The amount of double strained DNA (dsDNA), that is directly proportional with the cell number, was determined using a fluorometric dsDNA quantification kit (PicoGreen, Molecular Probes, Invitrogen, USA), according to the manufacturer's instructions. Samples collected at days 7, 14, 21 and 28 of culture were subjected to thermal and osmotic shocks to lyse the cells. Cell lysates were then used for the dsDNA quantification. Fluorescence was measured using an excitation wavelength of 480 nm and emission wavelength of 538 nm in a microplate reader (Synergy HT, Biotek, USA). Standards were prepared at a concentration ranging between 0 and 2 mg/mL. Triplicates were made for each sample and per condition.

2.7. Real-time reverse transcriptase-polymerase chain reaction (RT-PCR)

2.7.1. RNA extraction and cDNA production

mRNA was extracted using TRI Reagent→ (Sigma, Germany), following the manufacturer instructions. Proteins were extracted using chloroform and the RNA pellets were washed with isopropyl alcohol and 70% ethanol. The total mRNA was reconstituted in RNAse-free water (Gibco, USA). mRNA quantity and purity were assessed with a NanoDrop ND-1000 Spectrophotometer (NanoDrop Technologies, USA). First-stranded complementary DNA (cDNA) synthesis was performed using qScript™ cDNA synthesis Kit (Quanta BIosciences, USA) on a Mastercycler ep realplex thermal cycler (Eppendorf, USA). An initial amount of 1 μg of mRNA was used in a total volume of 20 μL.

2.7.2. Quantitative real time RT-PCR

The quantification of the transcripts of the genes of interest was carried out by RT-PCR using 50 ng of cDNA and PerfeCTA™ SYBR® Green FastMix kit (Quanta Biosciences, USA) following the procedure suggested by the manufacturer. The primers were previously designed using the Primer 3 online software (v0.4.0, Whitehead Institute, USA) and synthesized by MGW Biotech (Germany). For each sample, the transcripts expression data were normalized to *glyceraldehyde-3-phosphate-dehydrogenase (GAPDH)* as housekeeping gene. The primers sequences and annealing and annealing temperatures for bone-specific genes, *Runt-related transcription factor 2* (*RUNX2*), *osteocalcin* (*OCN*) and *osteopontin* (*OPN*), and for *GAPDH* are described in Table 1. A concentration of 100 nM of primer was used in a final volume of 20 μl of sample. Reactions were performed in a real-time Mastercycler ep realplex thermal cycler (Eppendorf, USA). The relative quantification of the targeted genes was performed using the $2^{-\Delta\Delta CT}$ method [22]. The transcripts expression data were first normalized against endogeneous *GAPDH* values and then against the values of hASCs cultured in basal or osteo medium, respectively for basal and osteo conditions.

2.8. Alkaline phosphatase activity quantification and staining

The alkaline phosphatase (ALP) activity was measured on the cell lysates obtained for dsDNA quantification, using an adapted end-point colorimetric procedure based on the p-nitrophenol (pNP) assay. Briefly, 20 μL of lysate were incubated with 80 μL p-nitrophenol phosphate solution (pNPP, 0.2% wt/v in 1 M diethanolamine, Fluka BioChemika, Austria). A calibration curve was prepared using the pNP standards (Sigma, Germany) with values ranging from 0 to 0.5 μmol/mL. The OD of the samples and standards was read at 405 nm, using a microplate reader (Synergy HT, Biotek, USA). Triplicates of each sample and standard were made, and the ALP activity was read off from the standard curve. Results were normalized against dsDNA results obtained for the same samples. The qualitative detection of ALP was performed by staining the fixed samples with nitro-blue tetrazolium/indolylphosphate (NBT/BCIP, Thermo Scientific, USA). Samples were visualized and images were acquired as described above.

2.9. Collageneous and non-collageneous protein staining and quantification

The presence and distribution of collagen and non-collagenous proteins within the extracellular matrix (ECM) were determined by differential staining with two dyes, Sirius Red and Fast Green. Sirius Red binds specifically to collagen, whereas

Table 1
Primer pair sequences for the studies genes.

Gene	Sequences		NCBI reference
	Forward (5′→3′)	Reverse (3′→5′)	
GAPDH	ACAGTCAGCCGCATC	GACAAGCTTCCCGTTCTCAG	NM_002046.4
RUNX2	TTCCAGACCAGCAGCACTC	CAGCGTCAACACCATCATTC	NM_001145920.1
OPN	GGGGACAACTGGAGTGAAAA	CCC ACAGACCCTTCCAAGTA	NM_001040058
OCN	CTGGAGAGGAGCAGAACTGG	GGCAGCGAGGTAGTGAAGAG	NM_099173

Fast Green stains the non-collagen proteins. As so, the effect of sNPs over the ECM deposition was assessed using the micro-assay kit (Chondrex, USA). Briefly, a mixture of 0.1% Sirius Red and 0.1% Fast Green solution saturated with picric acid was added to the fixed samples. After 30 min, the dye was removed and samples rinsed with distilled water. Stained samples were visualized and images were acquired as described above.

For the quantification the dyes were extracted from the stained samples using 0.05 M NaOH solution in methanol and the OD measured at 540 nm (Sirius Red) and 605 nm (Fast Green). The amount of collagenous and non-collageneous proteins was calculated according to the manufacturers indications and normalized against the dsDNA of the corresponding samples.

2.10. Immunocytochemistry for collagen I and II

Samples were washed and fixed with 10% formalin for 20 min, washed again with PBS and blocked with a 1.5% BSA/PBS solution. Cells were incubated for 1 h at room temperature with the primary antibodies, mouse anti-human collagen I (abcam, ab90395, UK) and mouse anti-human collagen II (abcam, ab34712, UK). All antibody dilutions were performed in 1.5% BSA/PBS. Upon this incubation, cells were washed three times with PBS and incubated with the appropriate secondary antibody, either goat anti-mouse Alexa Fluor 488 (Invitrogen, USA), or donkey anti-mouse Alexa Fluor 594 (Invitrogen, USA) diluted 1:500 in 1.5% BSA/PBS. Cell nuclei were counterstained with DAPI, at a 1:10,000 dilution in PBS. Negative control samples were prepared by replacing the primary antibody incubation with PBS. Samples were visualized and images were acquired as described above.

2.11. Alizarin Red staining and quantification

Staining with Alizarin Red was performed in order to assess calcium deposition. The cells were fixed with 10% formalin, for 20 min, and washed prior staining with PBS and, again with distilled water to remove any contaminating salts. A 2% (wt/v) Alizarin Red solution (Sigma, Germany) was added and 10 min after, the cells were washed with distilled water and imaged as previously described. Subsequently, in order to obtain quantitative data, the extraction of the dye from the stained cell monolayer was performed by the addition of a 10% (v/v) acetic acid (vWR, Portugal). The dissolved samples were transferred to microcentrifuge tubes, centrifuged and neutralized with 10% (v/v) ammonium hydroxide (Sigma, Germany). Finally, 100 μL of each sample was transferred in 96-well plate and the absorbance was read at 405 nm. A calibration curve was obtained from different concentrations of Alizarin Red in distilled water at pH = 4.2, adjusted with 10% (v/v) ammonium hydroxide.

2.12. Statistical analysis

Statistical analysis was performed using GraphPad Prism 5.00 software (San Diego, USA). Each experiment was carried out three times independently and performed with at least three replicates. First, a Shapiro–Wilk test was used to ascertain the data normality. The results indicated that non-parametric test should be employed for all comparisons. Statistical significances were determined using one-way analysis of variance (ANOVA), followed by post hoc Tukey test for all pair-wise mean comparisons, with the limit for statistical significance being defined as $p < 0.05$.

3. Results

3.1. SNPs characterization

Silicate nanoplateletes (sNPs) are synthetic disc-shaped crystals, characterized by a high aspect ratio (25–30 nm in diameter and 1 nm in width) and with an empirical formula given by $Na^{+}_{0.7}[(Si_8Mg_{5.4}Li_{0.3})O_{20}(OH)_4]^{-}_{0.7}$ (Fig. 2A). The unit cell of the crystal is comprised of layers of $[SiO_4]$ tetrahedral sheets of Mg^{2+}, which complement their octahedral coordination by bridging with OH^{-} groups. The partial substitution of Mg^{2+} in the octahedral sheets by Li^{+}, charges the faces of the sNPs negatively, so that Na^{+} ions are accommodated between the faces of the platelets for charge compensation, leading to a defined spatial distribution of charge on the sNPs [23]. When sNPs are dispersed in distilled water, the Na^{+} ions are released into the solution leading to the formation of a double layer that causes the particles to electrostatically repeal each other, hence stabilizing them in overall negative charge of 10–15 mV. However, with the increase of concentration (>100 μg/mL), a significant increase in the overall size of the sNPs,

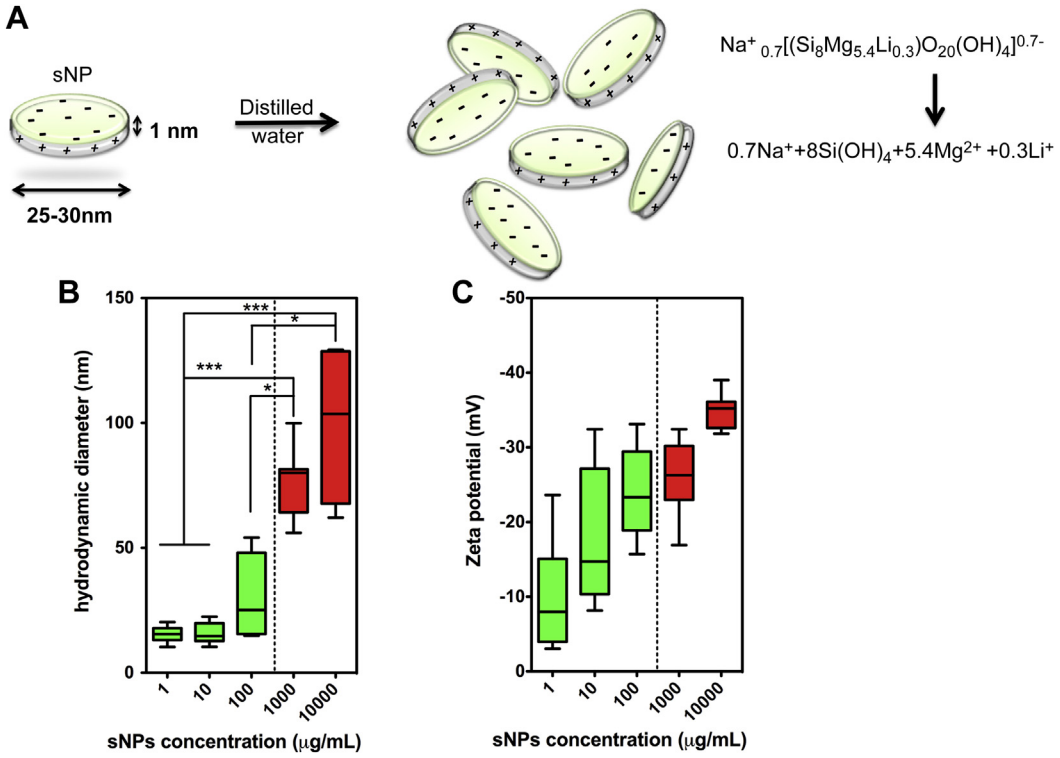

Fig. 2. Physical properties of the sNPs. (A) The sNPs, with the $Na^{+}_{0.7}[(Si_8Mg_{5.4}Li_{0.3})O_{20}(OH)_4]^{-}_{0.7}$ empirical formula, are characterized by a high aspect ratio (25:1 to 30:1) and charge distribution (negatively charged facets and positively charged sides). Due to surface charge, upon dispersion in distilled water, sNPs electrostatically repel each other, avoiding aggregation. (B–C) Box plots depicting the sNPs hydrodynamic diameter and zeta potential. In dilute suspension, the sNPs are well dispersed and negatively charged. However, at increased concentrations, strong van der Waals forces make the sNPs to adhere to each other, such as in the mechanism of flocculation or aggregation ($^{*}p < 0.05$, $^{**}p < 0.01$, $^{***}p < 0.001$).

accompanied by a slight decrease of the overall charge, was observed (Fig. 2B–C).

3.2. Cells and sNPs interactions and potential internalization mechanism

The potential cytotoxic effects of the sNPs were assessed after exposing the SSEA-4$^+$hASCs to different concentrations of sNPs over a period of 7 days. MTS test was performed to assess the metabolic activity of cells in the presence of sNPs. The addition of up to 100 μg/mL sNPs to the cells did not cause changes in their metabolic activity, however at concentrations (ranging from 250 to 10,000 μg/mL) an abrupt decrease in the metabolic activity of cells was observed (Fig. 3A). Moreover, SSEA-4$^+$hASCs cultured in the presence of sNPs at concentrations lower than 100 μg/mL displayed a homogeneous fibroblast-like morphology characteristic of mesenchymal cells (Fig. 3B and Supplemental Fig. 1). However, at high concentrations (>100 μg/mL), small sNPs clusters were observed on the surface of the cells. At those concentrations, cells were covered with a gel-like aggregate that lead to an apparent shrinkage of the cells cytoskeleton (Supplemental Fig. 1). Previous report also indicates that sNPs concentration of <100 μg/mL does not result in significant production of reactive oxygen species (ROS) and reactive nitrogen species (RNS), indicating the cytocompatible nature of sNPs [12]. Thus, for further experiments, it was decided not to consider sNPs concentrations higher than 100 μg/mL, as these lead to a reduction of cells metabolic activity greater than 20% and significant cellular morphological alterations.

Labeled sNPs were internalized and widely distributed in the cell cytoplasm, around the cells nuclei (Fig. 4A), but also attached to the cell membranes (Supplemental Fig. 1). In order to elucidate the internalization mechanism and deplete internalization from external contact of the cells with the sNPs, cells were cultured in the presence of rhodamine-labeled sNPs and colchicine, an endocytotic restrictive drug, for a period of 24 h. When cells were cultured in the absence of colchicine (green peak), a strong shift was observed, which is associated with cell-sNPs interaction derived from fluorescent sNPs externally attached to the cells, as well as internalized (Fig. 4B). At high concentration of sNPs (100–250 μg/mL), more than 80% of cells interacted with the sNPs. However, in the presence of colchicine, there was a noticeable decrease (white peak). At high concentrations, only 30% of the cells were positive (interacting with the sNPs). Considering the difference between the results with and without colchicine as the internalization efficiency, with the premise that the internalization of the sNPs is solely endocytotic, the internalization efficiency ranges from 5% for 1 μg/mL and can reach 40% for 100 μg/mL of sNPs (Fig. 4C).

3.3. SNPs effect on the SSEA-4$^+$hASCs osteogenic differentiation

Prior differentiation, SSEA-4$^+$hASCs were characterized as previously described [21] for the expression of surface markers such as CD105, CD90, CD73, CD45 and CD34. The cells showed mesenchymal-like phenotype, displaying the characteristic multiple-parametric pattern [24]: CD90$^+$/CD105$^+$/CD73$^+$/CD45$^-$/CD34$^-$ (Supplemental Fig. 2).

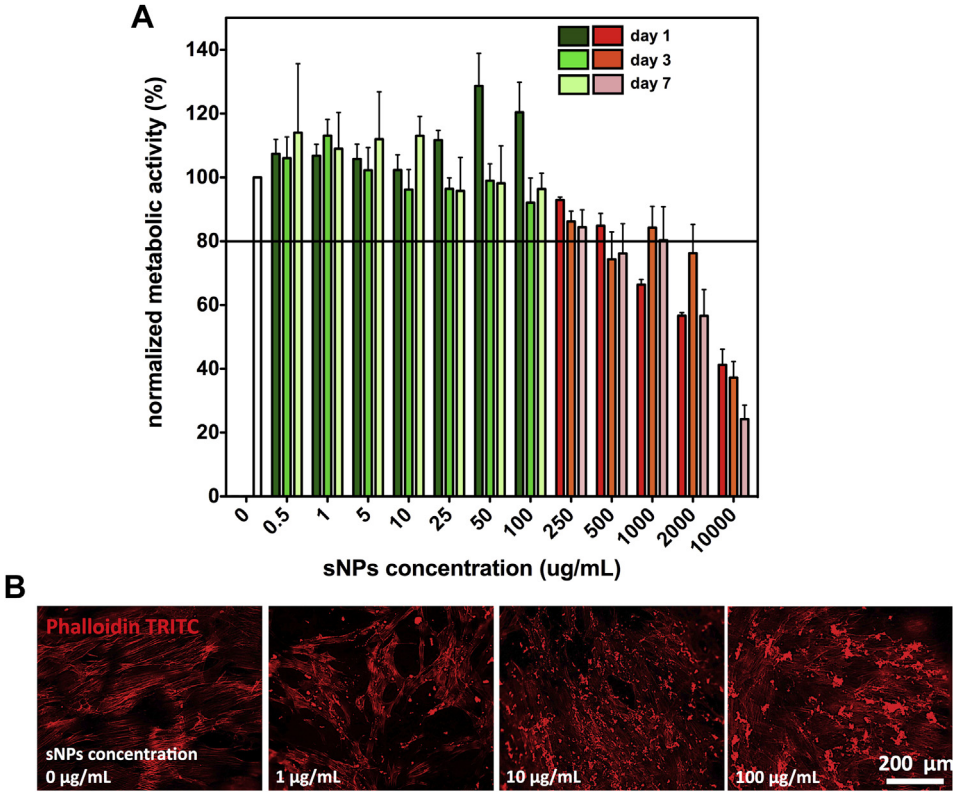

Fig. 3. Dependence of cellular behavior with sNPs concentration. (A) Metabolic activity of cells in the presence of different concentrations of sNPs. Results are presented as percentage of metabolic activity of SSEA-4$^+$hASCs in the presence of sNPs in relation to the metabolic activity of SSEA-4$^+$hASCs cultured without sNPs (control) at the considered time point (average ± SD, $n = 3$). The metabolic activity threshold for choosing the appropriate sNPs concentrations was set to 80% in relation to the control. The half maximal inhibitory activity (IC_{50}) was found at a concentration of 1 mg/mL. (B) Cytoskeleton (F-actin fibers) organization (red) upon addition of sNPs. The addition of sNPs (<100 μg/mL) does not alter the morphology of the cells. Small sNPs aggregates can be observed on the surface of the cells, for higher concentrations of the sNPs. (For interpretation of the references to color in this figure legend, the reader is referred to the web version of this article.)

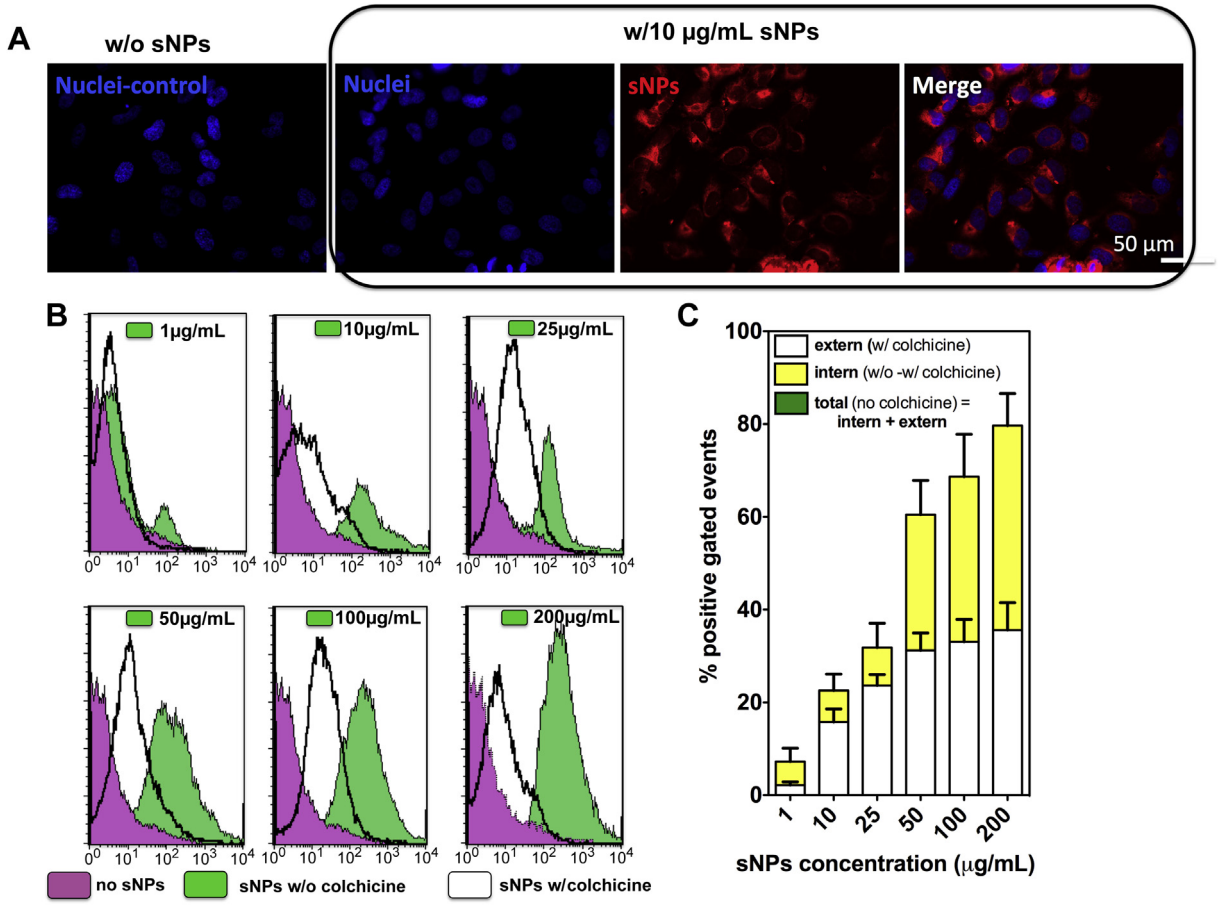

Fig. 4. Internalization of sNPs by SSEA-4$^+$hASCs. (A) Fluorescence microscopy images of cells cultured in the presence of rhodamine-labeled sNPs (red) for 24 h. Rhodamine-labeled sNPs were found distributed in the cell cytoplasm, around the cells nuclei (blue). (B) Flow cytometry data of cells interacting with the in the presence (white) or absence (green) of colchicine. Cells without sNPs were used as negative control (purple). (C) Quantification of the internalization (yellow) by subtracting the sNPs-cell interaction in the presence of colchicine (white) from the total sNPs-cell interaction (without colchicine, green). The internalization efficiency ranges from 5% for 1 μg/mL and can reach 40% for 100 μg/mL of sNPs. Abbreviation: w/ = with, w/o = without. (For interpretation of the references to color in this figure legend, the reader is referred to the web version of this article.)

3.3.1. The effect the expression of RUNX2, OPN and OCN transcripts in SSEA-4$^+$hASCs cultures

The acquisition of an osteogenic phenotype by SSEA-4$^+$hASCs when the culturing with sNPs was evaluated by following the expression levels of *RUNX2*, *OCN* and *OPN* genes. In basal medium, no fold changes were observed concerning any of the studied genes for SSEA-4$^+$hASCs, when compared to hASCs cultured in the same medium. However, with the addition of sNPs, a 2-fold increase for *RUNX2* and *OPN*, and of 8- for *OCN* was noticed ($^{***}p < 0.001$, Fig. 5A). For instance, a significant up-regulation of *RUNX2* occurred at day 7 for the higher sNPs concentration. This effect was successively delayed to days 14 and 21, when cells were cultured with 10 and 1 μg/mL sNPs, respectively. Concomitantly, the *OPN* expression is significantly increased at day 14 for the 10 and 100 μg/mL sNPs, followed by an immediate decrease to basal levels, while a significant up-regulation of *OCN* occurred at day 21 for all sNPs concentrations.

In osteogenic medium, there was a clear difference in the osteogenic performance between hASCs (control) and SSEA-4$^+$hASCs. A significant up-regulation of *RUNX2*, *OPN* and *OCN* gene transcripts was observed for SSEA-4$^+$hASCs ($^{**}p < 0.01$). After reaching a maximum (day 7 for *RUNX2*, day 14 for *OPN*, day 21 for *OCN*), a down-regulation reaching baseline levels of hASCs control cultures was observed (Fig. 5B). The addition of sNPs further increased the up-regulation of the genes of interest in such a manner that the 100 μg/mL sNPs induced a 70-fold increase ($^{*}p < 0.05$) in the expression of *RUNX2* at day 7, a 9-fold increase ($^{*}p < 0.01$) for *OPN* at day 14 and 45-fold increase ($^{*}p < 0.01$) for *OCN* at day 21 in relation to both the hASCs control cultures and SSEA-4$^+$hASCs in the absence of the sNPs.

3.3.2. The effect of sNPs over ALP activity

The osteogenic differentiation of the SSEA-4$^+$hASCs under the different culture conditions was confirmed, by qualitative and quantitative assessment of the levels of ALP activity, an early marker of differentiation, along the time of culture. ALP activity was confirmed in all groups, hASCs and SSEA-4$^+$hASCs, with and without sNPs, cultured in osteo medium. A clear increase of the ALP activity was evident up to 14 days of culture and for increased sNPs concentrations as demonstrated by the dark purple color (Fig. 6A). The quantitative analysis of ALP activity, normalized to the total dsDNA, confirmed the trend of these observations, with a 10-fold increase at day 14 (Fig. 6C). A slight increase of ALP activity occurred during initial time points, up to day 10, followed by a burst at day 14 ($^{*}p < 0.05$) and a successive rapid decrease at day 21. Additionally, the significantly higher ALP activity in SSEA-4$^+$hASCs ($^{*}p < 0.05$) when compared to hASCs cultured in the same conditions, and thus their enhanced predisposition to differentiate towards the osteogenic lineage, is noteworthy.

Concerning the cultures in basal medium, the constitutive ALP activity did not noticeably vary along the time of culture in both SSEA-4$^+$hASCs and hASCs. However, in the presence of sNPs the

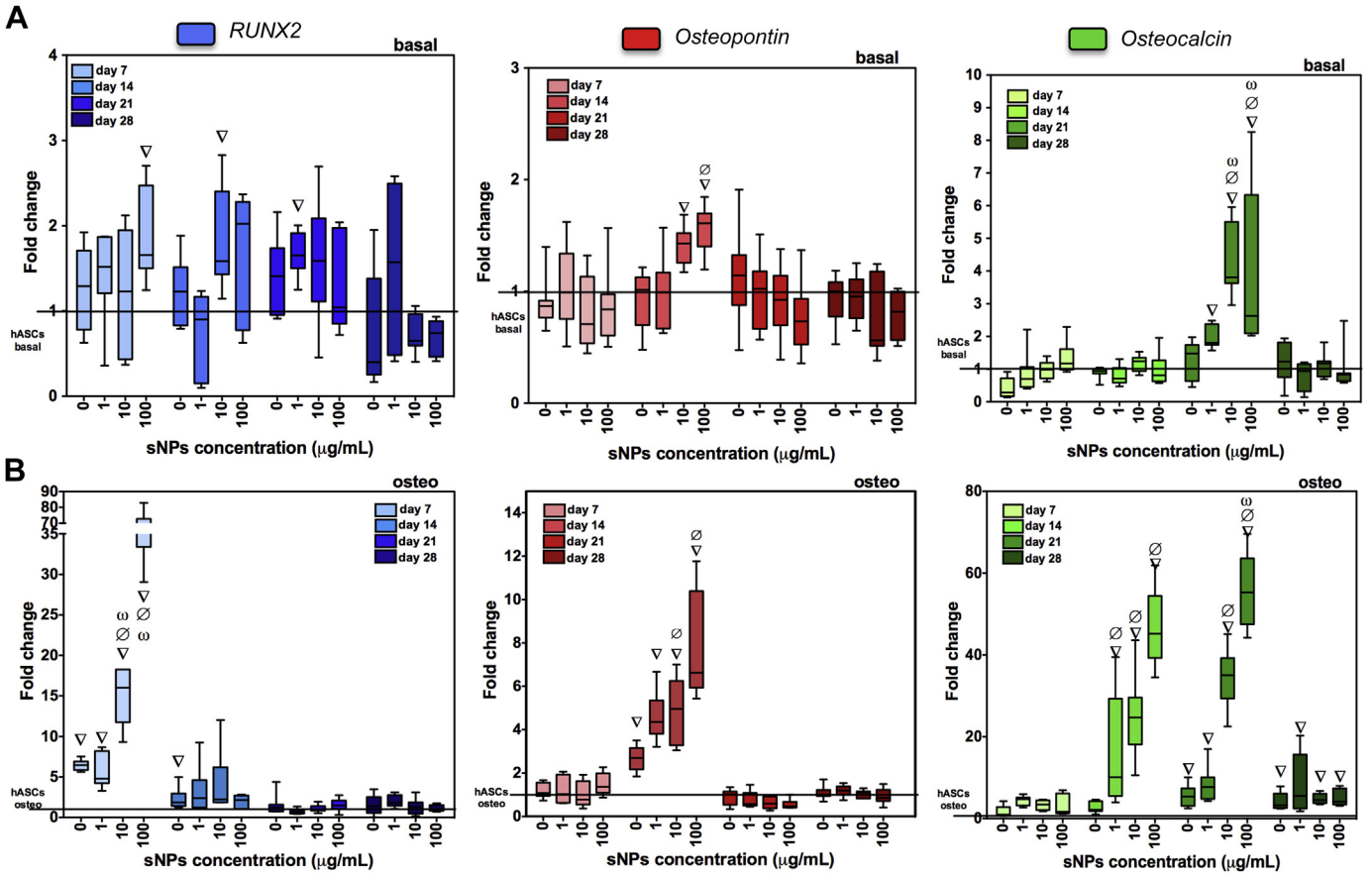

Fig. 5. RT-PCR results for early (*RUNX2*), intermediate (*OPN*) and late (*OCN*) osteo-related markers in SSEA-4$^+$hASCs cultures, in relation to hASCs cultures established in correspondent basal and osteogenic media. In basal medium (A) the expression of these transcripts is up-regulated in the presence of sNPs, in a dose-dependent manner, that also varies with the gene of interest. (B) Under osteogenic differentiation conditions, a significant increase in the expression of these markers was observed both in the absence and the presence of sNPs. A dependence with the sNPs concentration was observed for all the genes. ∇ depicts statistical difference ($^*p < 0.05$), when compared with hASCs group, ∅ corresponds to statistical differences when compared with SSEA-4$^+$hASCs without sNPs, while ω shows the statistical differences when compared with SSEA-4$^+$hASCs in the presence of 1 μg/mL sNPs.

ALP activity in the SSEA-4$^+$hASCs cultures increased as demonstrated by more intense staining at day 14, for the 10 and 100 μg/mL sNPs formulations (Fig. 6A). The quantitative analysis confirmed the observed trend. At day 14, a significant increase in ALP activity ($^*p < 0.05$) was observed for SSEA-4$^+$hASCs cultured with increasing concentrations of sNPs (Fig. 6B).

3.3.3. *The effect of sNPs over the deposition of collagenous proteins and matrix mineralization*

The deposition and distribution of the proteins that form the extracellular matrix was evaluated by Sirius Red/Fast Green staining, aiming at discriminating the collagenous from the non-collagenous proteins. When cells (hASCs and SSEA-4$^+$hASCs) were cultured in basal medium for 21 days, a uniformly distributed cyan coloration, corresponding to non-collagenous proteins, was observed. However, in the presence of sNPs, small purple regions, corresponding to collagen deposition, were observed. In osteogenic medium cultures, both in the presence and absence of sNPs, the cyan/purple ratio switched, so that large fibrillar-like collagenous regions overtook the regions that correspond to non-collagenous proteins. (Fig. 7A) The qualitative results were confirmed by the quantification of the total amount of collagen deposited in the different conditions. While no significant differences were observed in the amount of collagen deposited by hASCs and SSEA-4$^+$hASCs cultured in basal medium, the addition of sNPs led to significantly higher ($^*p < 0.05$) collagenous proteins deposition (Fig. 7B). Successively higher amounts were detected with increasing sNPs concentration reaching a nearly 8-fold in the presence of 100 μg/mL of sNPs. The SSEA-4$^+$hASCs cultured in osteogenic medium revealed a similar behavior, with cells being able to deposit a significantly higher amount of collagenous proteins ($^*p < 0.05$). The addition of 100 μg/mL sNPs to hASCs and SSEA-4$^+$hASCs resulted in a 3.4-fold and 2.1-fold increase, respectively when compared to cells cultured without sNPs (Fig. 7C). The quantification of non-collagenous proteins revealed constant levels of proteins both in basal and osteogenic media, except for the 100 μg/mL sNPs formulation in osteogenic medium which showed significantly higher values than the hASCs and SSEA-4$^+$hASCs cultured without sNPs (Supplemental Fig. 3A–B).

In order to determine the type of collagen composing the deposited collagenous matrix, the presence of collagen type I was evaluated at day 14, 21 and 28 by immunocytochemistry (Fig. 8). In basal media, only residual collagen type I was detected for both hASCs and SSEA-4$^+$hASCs. However, when sNPs were added to the SSEA-4$^+$hASCs, increased evidence of collagen type I was noticed. By day 28, only small collagen type I depots were identified in all conditions, including sNPs in basal medium. On the other hand, in osteogenic medium, collagen type I was dominantly present in all conditions. Moreover, an increased and uniformly distributed deposition seemed to be detected for the SSEA-4$^+$hASCs with the

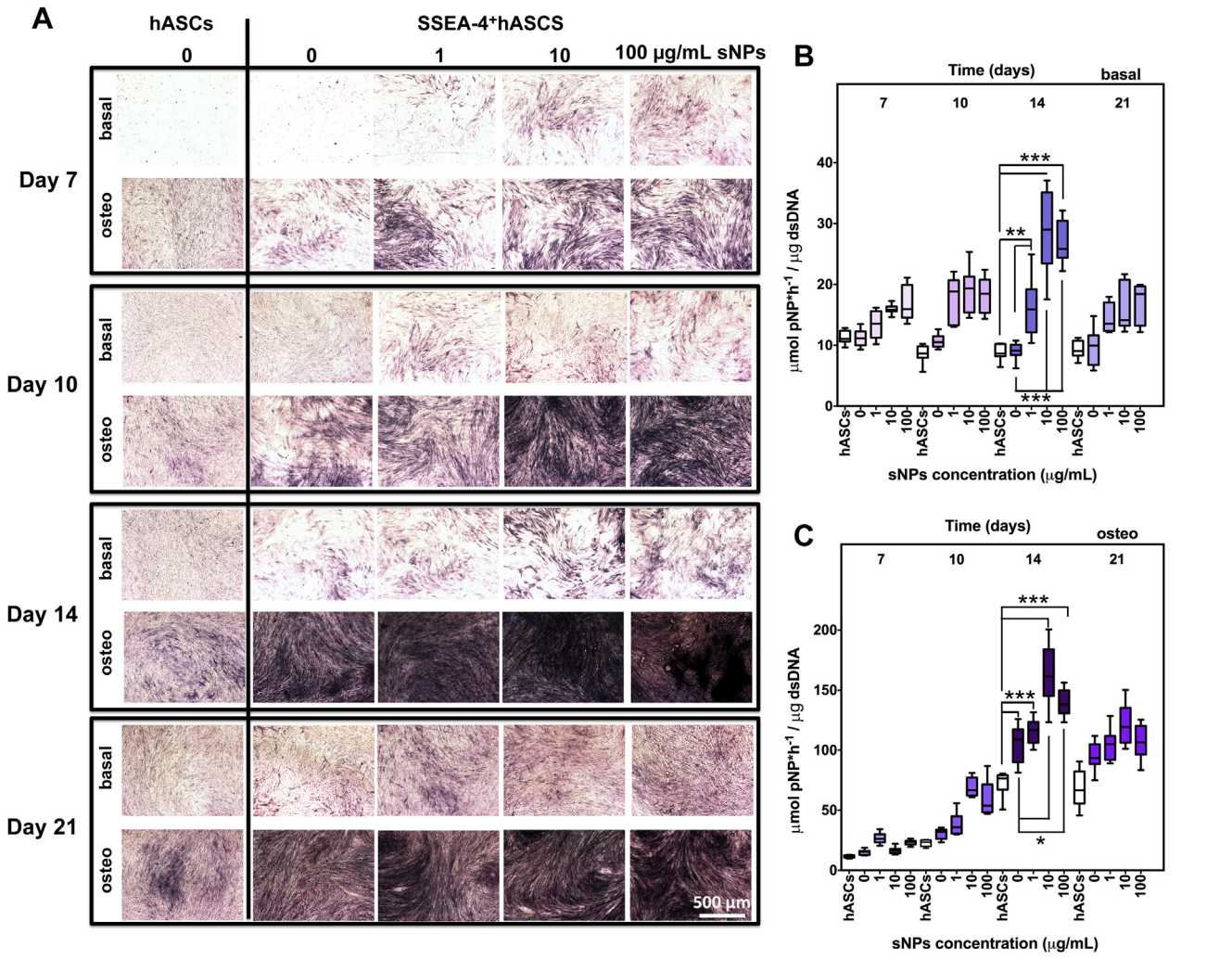

Fig. 6. Qualitative and quantitative analysis of alkaline phosphatase (ALP) activity during 21 days of culture. (A) NBT/BCIP staining (dark purple) highlights an intense coloration with the addition of sNPs, suggesting that the sNPs enhance ALP activity. (B–C) The presence of sNPs lead to significantly enhanced ALP activity at day 14 of culture in SSEA-4$^+$hASCs in basal and osteogenic media, when compared to hASCs cultured in the same conditions ($^*p < 0.05$, $^{**}p < 0.01$, $^{***}p < 0.001$). (For interpretation of the references to color in this figure legend, the reader is referred to the web version of this article.)

addition of sNPs. A similar trend was observed for collagen type II (Supplemental Fig. 3C). When the ratio between collagen type I and type II was analyzed, the highest percentage of collagen type I was found for the SSEA-4$^+$hASCs with 100 µg/mL of sNPs in osteogenic medium. Interestingly the highest percentage of collagen type II was found for SSEA-4$^+$hASCs treated with 100 µg/mL of sNPs in basal medium (Supplemental Fig. 3D).

Alizarin Red staining confirmed that in basal medium, matrix mineralization depots were only detected in the presence of sNPs (Fig. 9A). Moreover these significantly increased with increasing sNPs concentrations and longer time points (Fig. 9B). At day 28, the amount of inorganic calcium in the SSEA-4$^+$hASCs culture with sNPs was significantly higher ($^*p < 0.05$) than in the hASCs or SSEA-4$^+$hASCs cultures without sNPs. In osteogenic medium, significant mineral deposition was observed in the hASCs cultures as evidenced by the intensity of the staining. Nonetheless, SSEA-4$^+$hASCs cultures showed enhanced mineralization levels, with a more intense overall staining and higher number of mineralized regions in the presence of the sNPs (Fig. 9A). The extent of mineralization in osteogenic medium by day 28, 10-fold higher level than in basal medium, confirmed by significant differences ($^*p < 0.05$) between SSEA-4$^+$hASCs and hASCs cultures, both in the presence and absence of sNPs (Fig. 9C).

4. Discussion

One of the goals of bone TE is to design adequate supportive matrices for skeletal stem cells or progenitor cells to sustain the repair and regenerate damaged tissue. Focus has been given to AT as an alternative cell source to bone marrow MSCs [25]. At present, isolating homogenous stem cell subpopulations from the SVF of human AT that are more prone to differentiate into a certain lineage (osteogenic, chondrogenic, endothelial, etc) is being exploited as an approach to use this cell source more efficiently. So far CD49d$^+$hASCs [18], CD90$^+$hASCs [20] or CD105$^-$hASCs [19] were shown to possess an enhanced osteogenic differentiation potential when compared to unsorted cells (hASCs). However, as bone healing and regeneration relies on heterogeneous cellular interactions (eg. endothelial- and osteoblast-like cells), the use of a cell source/subpopulation with potential to differentiate towards these lineages relevant for bone tissue engineering might be advantageous. Our previous work [21] showed that besides being able

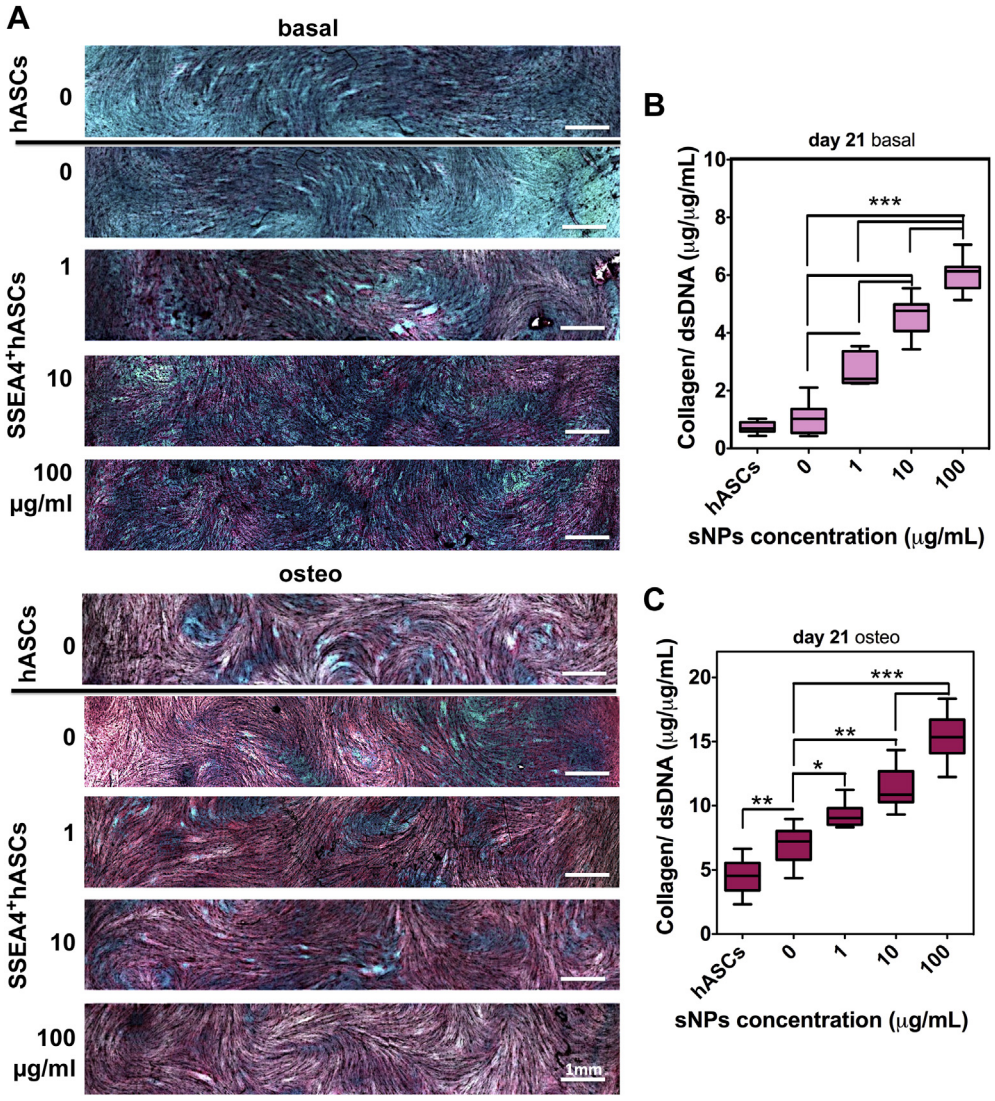

Fig. 7. Detection of proteins produced by hASCs and SSEA-4$^+$hASCs when cultured in basal and osteogenic media for 21 days. (A) Fast Green and Sirius Red staining depicts the distribution of collagenous (purple) and non-collagenous (cyan) proteins within the matrix. (B–C) Quantification of collagenous proteins normalized against the amount of dsDNA. The osteogenic differentiation of SSEA-4$^+$hASCs is characterized by a significantly enhanced collagen production in comparison to the hASCs. The addition of sNPs lead also to an increased production of collagenous proteins in both basal and osteogenic conditions ($^*p < 0.05$, $^{**}p < 0.01$, $^{***}p < 0.001$).(For interpretation of the references to color in this figure legend, the reader is referred to the web version of this article.)

to differentiate towards osteogenic lineage, the SSEA-4$^+$hASCs subpopulation residing within the SVF of the AT could differentiate into microvascular-like endothelial cells. This dual-differentiation potential features the possibility to obtain the relevant type of cells using a single-source and a single step-isolation procedure to engineer vascularized bone tissue.

Recently, the potential of sNPs (Laponite, $Na^+_{0.7}[(Si_8Mg_{5.4}Li_{0.3})O_{20}(OH)_4]^-_{0.7}$) to induce the osteogenic differentiation of bone marrow stromal cells in the absence of any external osteoinductive factors was demonstrated [12]. Thus, we herein propose the use of sNPs as instruments to promote and improve the osteogenic differentiation of SSEA-4$^+$hASCs.

Intrinsic and extrinsic properties of nanoparticles such as surface area, charge and functionalities, as well as size and shape, might impact cytotoxicity. Cytotoxicity tests were carried out considering the threshold of 20% reduction of SSEA-4$^+$hASCs metabolic activity. Our data is in agreement with previously published studies [12]: nanoparticles with negative zeta potential were shown to be significantly less internalized by cells than nanoparticles with positive zeta potential [26]. The cationic surface of sNPs is responsible for their interactions with the anionic glycoproteins and phospholipids of the cell membrane, which possibly facilitates their internalization [27]. This suggests that the cellular uptake occurs when sNPs are oriented with their positive side towards the cell membrane, ensuring a low area [28] and their engulfment and the disguise of the negative facet. However, the use of positively charged systems remains problematic *in vivo* as their interaction with negatively charged serum proteins and red blood cells may form large clusters and interfere with normal metabolic processes [29]. In fact, our *in vitro* data reproduced this observation, as for sNPs concentrations higher than 100 µg/mL, the formation of clusters that could hinder the internalization mechanism was observed. As a consequence, these clusters attached to the cell membrane, impairing cell cytoskeletal organization and metabolism. At the same time, it is known that the optimal nanoparticle diameter for cellular uptake is in the order of 25–30 nm [30], which is in good agreement with the radius reported for the sNPs [12,31], at concentrations below 100 µg/mL. In addition to being uptaken by

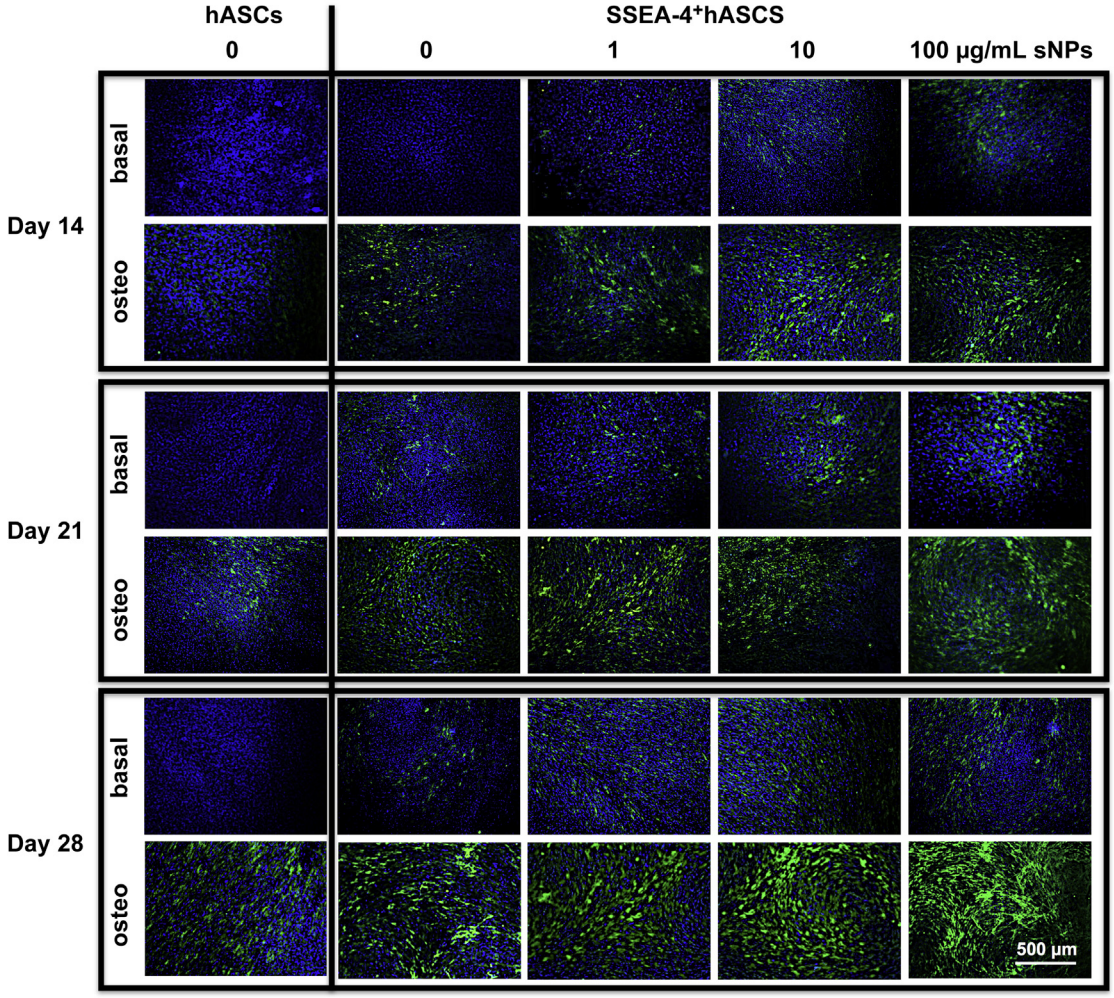

Fig. 8. Representative immunofluorescence images of the detection of collagen type I (green) over time and for the different experimental conditions. The addition of sNPs triggers the deposition of collagen type I in both basal and osteogenic media. Cell nuclei were counterstained with DAPI (blue). (For interpretation of the references to color in this figure legend, the reader is referred to the web version of this article.)

cells, as suggested by the rhodamine-labeled sNPs homogeneously localized around the cellular nuclei, sNPs were also found attached to the cellular membrane, without affecting the cells fibroblastic-like morphology. Therefore, the cells-sNPs interaction comprise the sum of the external contact at the membrane level, and of the internal effect, due to the engulfed sNPs. In order to isolate these two types of interactions, complementary experiments were carried out by inhibiting the endocytotic internalization mechanism using colchicine, an endocytotic restrictive drug. Colchicine is known to bind tightly to microtubules causing microtubule depolymerization, further affecting the endocytosis mechanism [27]. Based on the narrow sNPs range size, our hypothesis was that the cellular uptake predominately occurred *via* clathrin-mediated endocytosis pathway, as already reported elsewhere [30,32] (Supplemental Fig. 4). Our data suggests that the interactions that occur at the membrane level are equally important as the ones that occur internally. Particularly, it was possible to estimate that for the 100 µg/mL sNPs, both the cytoplasmic effect and external interactions have an equal contribution (approx. 35% each).

Independent of being entrapped within the endosome, attached to the cell membrane, or in suspension in the culture medium, particularly at low pH [31,33], sNPs are subjected to constant acidic and/or enzymatic degradation, dissociating into silicic acid ($Si(OH)_4$), Na^+, Mg^{2+} and Li^+. All of these were shown to improve the osteogenic differentiation by different mechanisms [34–36]. *In vitro* osteogenic differentiation is characterized by several temporal milestones that demonstrate the commitment of the cells towards the osteoblastic phenotype. At early stages of differentiation, the activation of the *RUNX2* transcription factor occurs to facilitate the convergence of numerous osteogenic signaling pathways [37,38]. Our data features an intense up-regulation of *RUNX2* for the SSEA-4^+hASCs cultured in osteogenic medium, in comparison to hASCs. Moreover, in the presence of sNPs a significantly higher up-regulation, proportional to the sNPs concentration, was observed which indicates that the osteogenic differentiation was triggered due to a signal provided by the sNPs. Interestingly, *RUNX2* expression up-regulation was also noted in basal medium at different time points for the different concentrations of sNPs. Earlier up-regulation was detected for higher sNPs concentration, which is in accordance to our previously published data that showed the osteogenic differentiation of bone marrow stromal cells in the absence of any external osteoinductive factors [12].

Considered to be the central control gene within the acquisition of osteoblast phenotype, *RUNX2* directly stimulates ALP activity [39] and the up-regulation of osteogenic-related genes such as *OPN* or *OCN* [38,40], and genes responsible for encoding collagenous-like matrix, mainly constituted of type I collagen [41], which is a prerequisite for mineralization [42,43]. The follow-up of

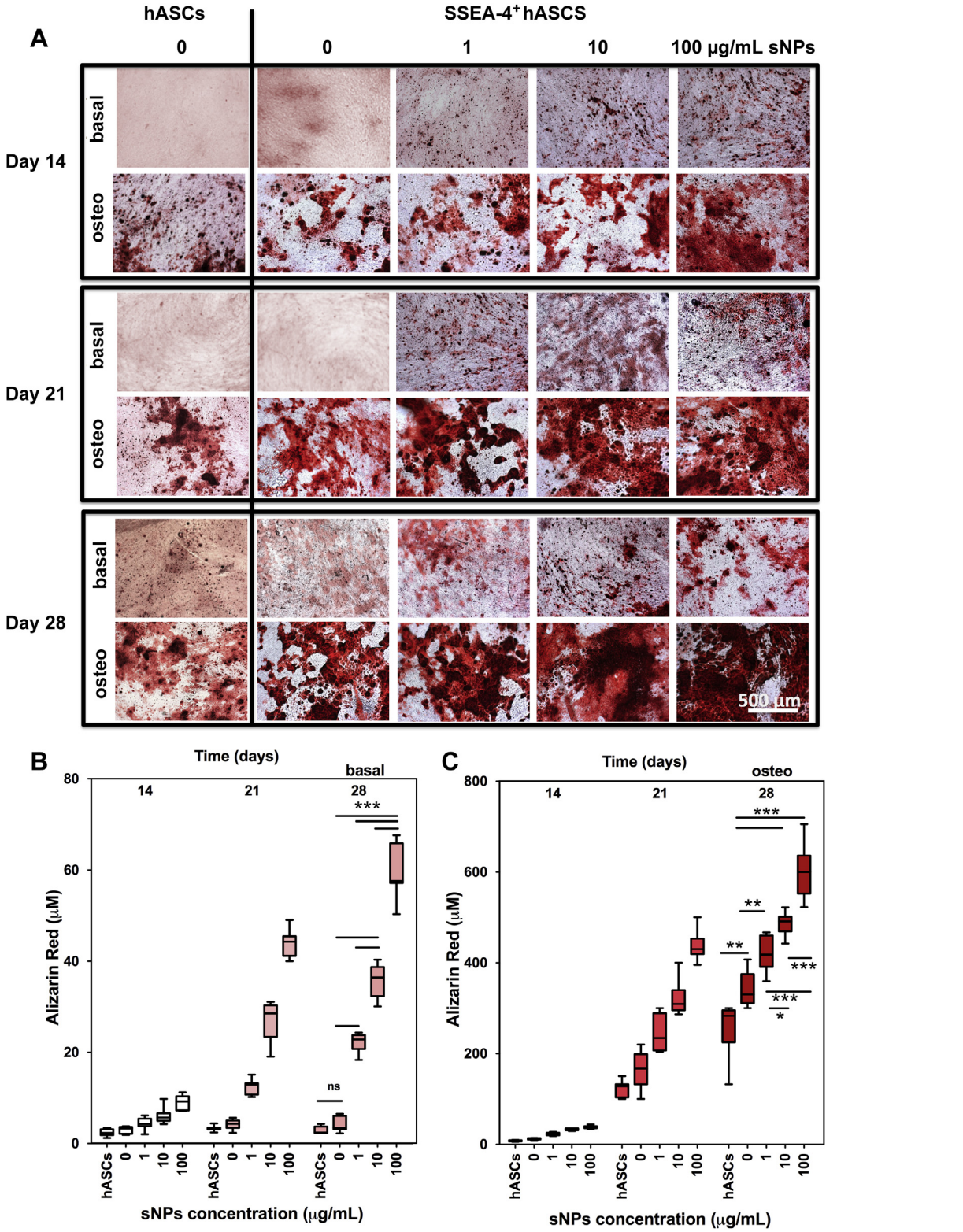

Fig. 9. Alizarin Red staining and respective quantification of the gradual mineralization of the deposited matrix along the culture. (A) Alizarin Red staining showed an intense coloration for increased sNPs concentrations. (B–C) Quantification of Alizarin Red staining confirmed a significant higher matrix mineralization in the SSEA-4$^+$hASCs cultures in the presence of sNPs, both in basal and osteogenic media ($^*p < 0.05$, $^{**}p < 0.01$, $^{***}p < 0.001$).

the temporal cascade of events after confirming *RUNX2* up-regulation, showed that the nature of the deposited matrix was dependent on the cell type and/or culture media and/or addition of sNPs. A maximum of ALP activity was detected, independent of the culture media, although at different levels, at day 14, as expected as an indication of the osteogenic phenotype acquisition [39,44]. As for *RUNX2* expression, sNPs alone lead to increased ALP activity; however, a plateau was reached when 10 µg/mL sNPs

were used. In opposition to *RUNX2*, the dependence of the *OPN* and *OCN* expression with the sNPs concentration did not affect its temporal profile. As expected during osteogenic differentiation [45], the maximum up-regulation of *OPN* transcripts was observed at day 14 while for *OCN* a peak was detected between days 14 and 21.

Among the dissociation products of sNPs, soluble silicate ions have been found to stimulate the expression of collagen type I in osteoblast-like cell cultures [3], while magnesium [35] and lithium [36,46] were shown to facilitate mineralization [43,47]. Thus, upon triggering the cells differentiation towards the osteogenic lineage, it was expected that the sNPs would also affect the nature of the deposited extracellular matrix (ECM). The deposition of collagenous-proteins, in detriment of non-collagenous proteins, gradually took over when SSEA-4$^+$hASCs were cultured together with sNPs, in basal medium, although the levels observed in osteogenic medium were not reached. As a general remark, collagen stained by Sirius Red displayed a fibrillar pattern, whereas non-collagen proteins stained with Fast Green showed a more diffused pattern. In fact, the deposited matrix under osteogenic conditions was mainly composed of collagen type I, known to be produced by developing osteoblast-like cells and an early indicator of the osteogenic differentiation [43], a prevalence of collagen II was detected when cells were cultured in basal medium.

Different works have shown that the enzymatic activity of ALP has a direct role in initiating the calcification process [39,48,49]. Taken together, the ALP enriched cuboid-shaped clusters, the pattern of collagen deposition and the Alizarin Red staining, confirmed the conclusion of the differentiation process. This was achieved with greater efficiency for the SSEA-4$^+$hASCs cultures in the presence of sNPs under osteogenic conditions, as demonstrated by more than 90% of the culture area depicting the formation of new mineralized nodules. Nonetheless, the SSEA-4$^+$hASCs cultures in basal medium with presence of sNPs also generated calcium depots, indicating successful differentiation of SSEA-4$^+$hASCs into osteoblast-like cells, although at lower rates than in osteogenic conditions. Therefore, by applying a single dose of sNPs to cells with high osteogenic differentiation potential promotes up-regulation of bone-related markers, which lead to production of enhanced mineralized matrix.

5. Conclusions

By means of immunomagnetic selection targeting the SSEA-4 surface marker, it is possible to select a subpopulation with high differentiation potential (SSEA-4$^+$hASCs). Our data suggest that the SSEA-4$^+$hASCs bear higher osteogenic differentiation potential than hASCs, which can be further enhanced by the addition of sNPs in a dose dependent manner. Thus, envisioning bone tissue regeneration, the association of SSEA-4$^+$hASCs with sNPs harbors great potential in a TE approach towards the development of highly mineralized templates using an independent differentiation process. Even more, this unique combination can be further exploited in association with endothelial derived SSEA-4$^+$hASCs and 3D-templates to design improved bone analogs.

Acknowledgments

Authors thank the Portuguese Foundation for Science and Technology (FCT) for the personal grant SFRH/BD/42968/2008 through the MIT-Portugal Program (SMM). The research leading to these results has received funding from the MIT/ECE/0047/2009 project and the European Union's Seventh Framework Programme (FP7/2007-2013) under grant agreement n°REGPOT-CT2012-316331-POLARIS and MIT/ECE/0047/2009 project.

Appendix A. Supplementary data

Supplementary data related to this article can be found at http://dx.doi.org/10.1016/j.biomaterials.2014.07.052.

References

[1] Muller P, Bulnheim U, Diener A, Luthen F, Teller M, Klinkenberg ED, et al. Calcium phosphate surfaces promote osteogenic differentiation of mesenchymal stem cells. J Cell Mol Med 2008;12:281–91.
[2] Barradas AM, Monticone V, Hulsman M, Danoux C, Fernandes H, Tahmasebi Birgani Z, et al. Molecular mechanisms of biomaterial-driven osteogenic differentiation in human mesenchymal stromal cells. Integr Biol 2013;5:920–31.
[3] Reffitt DM, Ogston N, Jugdaohsingh R, Cheung HF, Evans BA, Thompson RP, et al. Orthosilicic acid stimulates collagen type 1 synthesis and osteoblastic differentiation in human osteoblast-like cells in vitro. Bone 2003;32:127–35.
[4] Gaharwar AK, Peppas NA, Khademhosseini A. Nanocomposite hydrogels for biomedical applications. Biotechnol Bioeng 2014;11:441–53.
[5] Dawson JI, Oreffo RO. Clay: new opportunities for tissue regeneration and biomaterial design. Adv Mater 2013;25:4069–86.
[6] Gaharwar AK, Mihaila SM, Swami A, Patel A, Sant S, Reis RL, et al. Bioactive silicate nanoplatelets for osteogenic differentiation of human mesenchymal stem cells. Adv Mater 2013;25:3329–36.
[7] Goncalves G, Cruz SM, Ramalho A, Gracio J, Marques PA. Graphene oxide versus functionalized carbon nanotubes as a reinforcing agent in a PMMA/HA bone cement. Nanoscale 2012;4:2937–45.
[8] Gaharwar AK, Kishore V, Rivera C, Bullock W, Wu CJ, Akkus O, et al. Physically crosslinked nanocomposites from silicate-crosslinked PEO: mechanical properties and osteogenic differentiation of human mesenchymal stem cells. Macromol Biosci 2012;12:779–93.
[9] Gaharwar AK, Schexnailder P, Kaul V, Akkus O, Zakharov D, Seifert S, et al. Highly extensible bio-nanocomposite films with direction-dependent properties. Adv Funct Mater 2010;20:429–36.
[10] Gaharwar AK, Schexnailder PJ, Dundigalla A, White JD, Matos-Pérez CR, Cloud JL, et al. Highly extensible bio-nanocomposite fibers. Macromol Rapid Commun 2011;32:50–7.
[11] Gaharwar AK, Schexnailder PJ, Jin Q, Wu C-J, Schmidt G. Addition of chitosan to silicate cross-linked PEO for tuning osteoblast cell adhesion and mineralization. ACS Appl Mater Interfaces 2010;2:3119–27.
[12] Gaharwar AK, Mukundan S, Karaca E, Dolatshahi-Pirouz A, Patel A, Rangarajan K, et al. Nanoclay-enriched poly (ε-caprolactone) electrospun Scaffolds for osteogenic differentiation of human mesenchymal stem cells. Tissue Eng Part A 2014. http://dx.doi.org/10.1089/ten.tea.2013.0281.
[13] Gaharwar AK, Schexnailder PJ, Kline BP, Schmidt G. Assessment of using Laponite cross-linked poly (ethylene oxide) for controlled cell adhesion and mineralization. Acta Biomater 2011;7:568–77.
[14] Zuk PA, Zhu M, Ashjian P, De Ugarte DA, Huang JI, Mizuno H, et al. Human adipose tissue is a source of multipotent stem cells. Mol Biol Cell 2002;13:4279–95.
[15] Schaffler A, Buchler C. Concise review: adipose tissue-derived stromal cells–basic and clinical implications for novel cell-based therapies. Stem Cells 2007;25:818–27.
[16] Zuk PA, Zhu M, Mizuno H, Huang J, Futrell JW, Katz AJ, et al. Multilineage cells from human adipose tissue: implications for cell-based therapies. Tissue Eng 2001;7:211–28.
[17] Anghileri E, Marconi S, Pignatelli A, Cifelli P, Galie M, Sbarbati A, et al. Neuronal differentiation potential of human adipose-derived mesenchymal stem cells. Stem Cells Dev 2008;17:909–16.
[18] Rada T, Reis RL, Gomes ME. Distinct stem cells subpopulations isolated from human adipose tissue exhibit different chondrogenic and osteogenic differentiation potential. Stem Cell Rev 2011;7:64–76.
[19] Levi B, Wan DC, Glotzbach JP, Hyun J, Januszyk M, Montoro D, et al. CD105 protein depletion enhances human adipose-derived stromal cell osteogenesis through reduction of transforming growth factor beta1 (TGF-beta1) signaling. J Biol Chem 2011;286:39497–509.
[20] Chung MT, Liu C, Hyun JS, Lo DD, Montoro DT, Hasegawa M, et al. CD90 (Thy-1)-positive selection enhances osteogenic capacity of human adipose-derived stromal cells. Tissue Eng Part A 2013;19:989–97.
[21] Mihaila SM, Frias AM, Pirraco RP, Rada T, Reis RL, Gomes ME, et al. Human adipose tissue-derived SSEA-4 subpopulation multi-differentiation potential towards the endothelial and osteogenic lineages. Tissue Eng Part A 2013;19:235–46.
[22] Pfaffl MW. A new mathematical model for relative quantification in real-time RT-PCR. Nucleic Acids Res 2001;29:e45.
[23] Lezhnina MM, Grewe T, Stoehr H, Kynast U. Laponite blue: dissolving the insoluble. Angew Chem 2012;51:10652–5.
[24] Bourin P, Bunnell BA, Casteilla L, Dominici M, Katz AJ, March KL, et al. Stromal cells from the adipose tissue-derived stromal vascular fraction and culture expanded adipose tissue-derived stromal/stem cells: a joint statement of the International Federation for Adipose Therapeutics and Science (IFATS) and the International Society for Cellular Therapy (ISCT). Cytotherapy 2013;15:641–8.

[25] Izadpanah R, Trygg C, Patel B, Kriedt C, Dufour J, Gimble JM, et al. Biologic properties of mesenchymal stem cells derived from bone marrow and adipose tissue. J Cell Biochem 2006;99:1285–97.
[26] Gratton SE, Ropp PA, Pohlhaus PD, Luft JC, Madden VJ, Napier ME, et al. The effect of particle design on cellular internalization pathways. Proc Natl Acad Sci U S A 2008;105:11613–8.
[27] Jevprasesphant R, Penny J, Jalal R, Attwood D, McKeown NB, D'Emanuele A. The influence of surface modification on the cytotoxicity of PAMAM dendrimers. Int J Pharm 2003;252:263–6.
[28] Herd H, Daum N, Jones AT, Huwer H, Ghandehari H, Lehr CM. Nanoparticle geometry and surface orientation influence mode of cellular uptake. ACS Nano 2013;7:1961–73.
[29] Hillaireau H, Couvreur P. Nanocarriers' entry into the cell: relevance to drug delivery. Cell Mol Life Sci 2009;66:2873–96.
[30] Zhang S, Li J, Lykotrafitis G, Bao G, Suresh S. size-dependent endocytosis of nanoparticles. Adv Mater 2009;21:419–24.
[31] Ruzicka B, Zulian L, Ruocco G. More on the phase diagram of Laponite. Langmuir 2006;22:1106–11.
[32] Rejman J, Oberle V, Zuhorn IS, Hoekstra D. Size-dependent internalization of particles via the pathways of clathrin- and caveolae-mediated endocytosis. Biochem J 2004;377:159–69.
[33] Shahin A, Joshi YM. Physicochemical effects in aging aqueous Laponite suspensions. Langmuir 2012;28:15674–86.
[34] Zhai W, Lu H, Wu C, Chen L, Lin X, Naoki K, et al. Stimulatory effects of the ionic products from Ca-Mg-Si bioceramics on both osteogenesis and angiogenesis in vitro. Acta Biomater 2013;9:8004–14.
[35] Gu H, Guo F, Zhou X, Gong L, Zhang Y, Zhai W, et al. The stimulation of osteogenic differentiation of human adipose-derived stem cells by ionic products from akermanite dissolution via activation of the ERK pathway. Biomaterials 2011;32:7023–33.
[36] Satija NK, Sharma D, Afrin F, Tripathi RP, Gangenahalli G. High throughput transcriptome profiling of lithium stimulated human mesenchymal stem cells reveals priming towards osteoblastic lineage. PloS One 2013;8:e55769.
[37] Gersbach CA, Le Doux JM, Guldberg RE, Garcia AJ. Inducible regulation of Runx2-stimulated osteogenesis. Gene Ther 2006;13:873–82.
[38] Ducy P, Zhang R, Geoffroy V, Ridall AL, Karsenty G. Osf2/Cbfa1: a transcriptional activator of osteoblast differentiation. Cell 1997;89:747–54.
[39] Takahashi T. Overexpression of Runx2 and MKP-1 stimulates transdifferentiation of 3T3-L1 preadipocytes into bone-forming osteoblasts in vitro. Calcif Tissue Int 2011;88:336–47.
[40] Harada H, Tagashira S, Fujiwara M, Ogawa S, Katsumata T, Yamaguchi A, et al. Cbfa1 isoforms exert functional differences in osteoblast differentiation. J Biol Chem 1999;274:6972–8.
[41] Kern B, Shen J, Starbuck M, Karsenty G. Cbfa1 contributes to the osteoblast-specific expression of type I collagen genes. J Biol Chem 2001;276:7101–7.
[42] Eijken M, Koedam M, van Driel M, Buurman CJ, Pols HA, van Leeuwen JP. The essential role of glucocorticoids for proper human osteoblast differentiation and matrix mineralization. Mol Cell Endocrinol 2006;248:87–93.
[43] Lees S. Mineralization of type I collagen. Biophys J 2003;85:204–7.
[44] Jaiswal N, Haynesworth SE, Caplan AI, Bruder SP. Osteogenic differentiation of purified, culture-expanded human mesenchymal stem cells in vitro. J Cell Biochem 1997;64:295–312.
[45] Kirkham GR, Cartmell SH. Genes and proteins involved in the regulation of osteogenesis. In: Ashammakhi N, Reis R, Chiellini E, editors. Topics in tissue engineering; 2007. p. 3.
[46] Zamani A, Omrani GR, Nasab MM. Lithium's effect on bone mineral density. Bone 2009;44:331–4.
[47] Buxton PG, Bitar M, Gellynck K, Parkar M, Brown RA, Young AM, et al. Dense collagen matrix accelerates osteogenic differentiation and rescues the apoptotic response to MMP inhibition. Bone 2008;43:377–85.
[48] Bellows CG, Aubin JE, Heersche JN. Initiation and progression of mineralization of bone nodules formed in vitro: the role of alkaline phosphatase and organic phosphate. Bone Min 1991;14:27–40.
[49] Orimo H, Shimada T. The role of tissue-nonspecific alkaline phosphatase in the phosphate-induced activation of alkaline phosphatase and mineralization in SaOS-2 human osteoblast-like cells. Mol Cell Biochem 2008;315:51–60.